Crossover from fingering to fracturing in deformable disordered media

Ran Holtzman and Ruben Juanes*

Massachusetts Institute of Technology, 77 Massachusetts Avenue, Building 48-319, Cambridge, Massachusetts 02139, USA

(Received 3 March 2010; revised manuscript received 13 September 2010; published 14 October 2010)

We investigate the displacement of one fluid by another in a deformable medium with pore-scale disorder. We develop a model that captures the dynamic pressure redistribution at the invasion front and the feedback between fluid invasion and microstructure rearrangement. Our results suggest how to collapse the transition between invasion percolation and viscous fingering in the presence of quenched disorder. We predict the emergence of a fracturing pattern for sufficiently deformable media, in agreement with observations of drainage in granular material. We identify a dimensionless number that appears to govern the crossover from fingering to fracturing.

DOI: 10.1103/PhysRevE.82.046305 PACS number(s): 47.56.+r, 46.50.+a, 47.20.−k, 47.54.−r

The displacement of one fluid by another in disordered media—such as porous media, etched micromodels, nanopatterned surfaces, or biological tissues—gives rise to complex invasion patterns [1]. The classical phase diagram of fluid-fluid displacement delineates three different regimes [2]: compact displacement, capillary fingering (CF) or invasion percolation [3], and viscous fingering (VF) [4–6]. This classification, which is based on micromodel experiments and modified invasion percolation models, is applicable to drainage in rigid media under negligible gravity effects. Much attention has been devoted to the characterization of each regime, as well as the transition among the different regimes [7–10]. It has been shown, for instance, that pore-scale disorder in rigid media impacts the regime transition from invasion-percolation to VF [7,10].

Coupled fluid and granular flow also lead to a variety of patterns, including fractures [11], viscous fingers [12], desiccation cracks [13], and labyrinth structures [14]. The formation of these patterns typically involves large particle rearrangements. Interestingly, a transition from VF to fracturing (FR) has been observed for fluid displacement in viscoelastic fluids and colloidal suspensions [15,16]. This crossover depends on the system deformability and on the Deborah number—a ratio of the characteristic times of a flow event and viscoelastic relaxation [15].

The fracturing process in a disordered medium has been studied at length [13]. Block-spring network models that simulate fracture growth have emphasized the role of heterogeneity in the mechanical properties (elasticity or strength of the springs), using either annealed disorder [17,18] or quenched disorder [19,20]. However, the transition from fluid instability (capillary or viscous fingering) to fracturing remains poorly characterized at the pore scale. Recent modeling results suggest that the mode of gas invasion in a porous medium shifts from capillary invasion to fracture opening as the grain size decreases [21], in agreement with observations of gas bubble growth in sediments [22], and drying in three-dimensional granular media [23].

In this paper, we investigate the crossover from fingering to fracturing patterns in deformable disordered media by means of a pore-scale model of the displacement of one fluid by another. Our pore-scale model captures the dynamics of pressure redistribution at the invading front, allowing us to characterize the effect of the initial disorder in hydraulic properties on the transition from capillary to viscous fingering. The model incorporates the two-way coupling between fluid displacement and mechanical deformation, providing the mechanisms for pore opening in response to pressure loading (direct coupling), and alteration of the flow properties by particle rearrangements (reverse coupling). Despite its simplicity, the model predicts the emergence of fracture opening as a dominant feature of the invasion pattern for sufficiently deformable systems.

We develop a two-dimensional (2D) discrete model of a random medium. Since we are interested in elucidating the general mechanisms of fluid invasion, rather than performing predictions for a particular type of medium, we assume a simple square-lattice arrangement of dented blocks [Fig. 1(a)]. Variation in particle shapes leads to disorder in throat apertures, which is assumed to be uncorrelated in space. Mechanical interaction among the particles is represented through a block-and-spring model. The springs are assumed to be prestressed under compression, with sufficiently large confinement to prevent large microstructural rearrangements.

We construct two interacting networks, a solid network and a fluid network, whose nodes are the solid particles and the pore bodies, respectively. We solve for particle displacements and fluid pressures at the pore bodies. The characteristic length scale is the pore size a, which we take here as half the distance between nodes in the lattice. We model pore-scale disorder by assigning different initial area A and permeability k to the throats between pore bodies. Both the throat area and permeability scale with the square of the throat aperture r, that is, $A \sim r^2$, $k \sim r^2$. We characterize the disorder in throat aperture by drawing values from a uniform distribution, $r \in [1-\lambda, 1+\lambda]\bar{r}$, where $\bar{r} \sim a$. The coefficient $\lambda \in (0,1)$ is a measure of the degree of disorder [7].

We simulate the invasion of an inviscid nonwetting fluid into a medium initially saturated with a wetting fluid of dynamic viscosity μ. The inviscid fluid pressure is spatially uniform. A fluid-fluid interface will advance from one pore to another if the capillary pressure (the difference between

*juanes@mit.edu

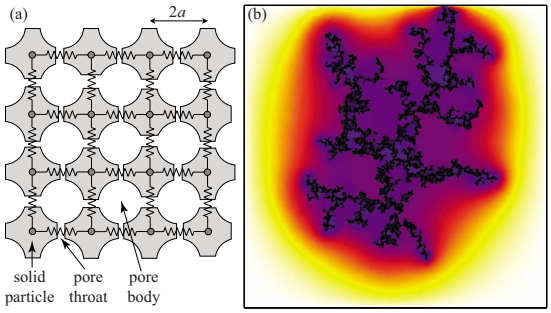

FIG. 1. (Color online) (a) Schematic of the model and simulation of drainage. The solid matrix is represented by a square lattice of dented blocks, connected mechanically by springs. The narrow openings between particles are the pore throats, which connect the larger openings (pore bodies). (b) An inviscid nonwetting fluid is injected at the center of the network, displacing a viscous wetting fluid. The pressure halo that surrounds the ramified invaded region reflects the finite time scale required for pressure dissipation in the defending fluid. The color scheme represents the logarithm of pressure normalized by the invading fluid pressure. In all our simulations, we use networks of 400×400 pores ($L=400a$) and set $a=0.1$ μm, $\mu=10^{-3}$ Pa s, $\gamma=0.07$ N m^{-1}, and $\epsilon_0=0.05$. Here, Ca $=9\times10^{-4}$ and $\lambda=0.3$.

nonwetting and wetting phase pressures) exceeds the capillary entry pressure $2\gamma/r$, where γ is the interfacial tension between the fluids and r is the aperture of the connecting throat [24]. If both fluids are inviscid, pressure variations in response to interface movement dissipate instantaneously; then, the process is described by the classical invasion-percolation algorithm [3] and depends exclusively on the quenched disorder.

Consideration of fluid viscosity introduces spatial nonlocality due to redistribution of the defending fluid along the invasion front. Slow drainage in disordered media occurs in the form of bursts, which lead to sudden changes in the defending fluid pressure ("Haines jumps" [25]). When one or more pores are drained during a burst, the interface menisci at neighboring pores readjust, receding along throats or even leading to a backfilling of previously drained pores [23]. The short time scales associated with pressure buildup in the defending fluid relative to that of drainage out of the system make fluid redistribution along the front a crucial mechanism [23,26,27]. This mechanism reduces the capillary pressure (the local curvature decreases as the meniscus recedes) and suppresses further invasion until the excess pressure in the defending fluid is dissipated, thus limiting the burst size.

Incorporating meniscus readjustments in a dynamic pore-network model [28,29] is computationally intensive. Here, we introduce the main effect of front interface dynamics: an effective compressibility of the system, even though the defending fluid is nearly incompressible.

The effective compressibility c_t can be obtained by the following argument. The capillary number is a ratio of viscous forces over capillary forces at the pore scale, Ca $=\Delta p_{\rm visc}/\Delta p_{\rm cap}$. Assuming Poiseuille flow, the viscous pressure drop over a pore length is $\Delta p_{\rm visc}\sim\mu v a/k$, with $k\sim a^2$ and v as the average flow velocity evaluated from the cumulative values of the drained volume, time, and cross-sectional area along the boundaries [27]. Together with the Young-Laplace equation, $\Delta p_{\rm cap}\sim\gamma/a$, this leads to the classical definition Ca$=\mu v/\gamma$. An alternative definition is the ratio of time scales for pressure dissipation and pore filling [27], Ca$'=\Delta t_{\rm press}/\Delta t_{\rm fill}$. Unlike [27], here we invoke pore-scale quantities only. The time scale for pressure dissipation is $\Delta t_{\rm press}\sim a^2/D$, where $D=(k/\mu)/c_t$ is the hydraulic diffusivity. The pore filling time scale is simply $\Delta t_{\rm fill}\sim a/v$, leading to Ca$'=(\mu v/\gamma)(c_t\gamma/a)$. Equating the two definitions of the capillary number provides the effective compressibility of slow drainage in a disordered medium:

$$c_t=\frac{a}{\gamma}. \tag{1}$$

In our simulations, the nonwetting fluid is injected at the center of the lattice at an approximately constant volumetric injection rate. Since the invading fluid is inviscid, we focus on the pressure evolution in the defending fluid. From mass conservation at a pore body, we write the equation of pressure evolution at an undrained pore, $p(t+\Delta t)=p(t)+\Sigma_j q_j\Delta t/(c_t V)$, where Δt is the time step, V is the pore volume, and the summation is over all neighboring pores. The volumetric flow rate between the pore and its neighbor j is given by Darcy's law $q_j=(Ak/\mu)(p_j-p)/\ell_j$, where ℓ_j is the length over which the pressure drop p_j-p is applied. For flow between two undrained pores, $\ell=2a$. If pore j is drained, the meniscus between the two pores starts advancing if $p_j-p>2\gamma/r$. The consequent pressure variations in the undrained pore are governed by the ability of the medium to dissipate pressure through the effective compressibility. The length over which viscous pressure drop takes place decreases as the meniscus advances, according to the expression $\ell_j(t+\Delta t)=\ell_j(t)-(q_j/A)\Delta t$.

A typical invasion pattern from our model for conditions near the transition between CF and VF is shown in Fig. 1(b). The simulation clearly shows the presence of a pressure halo surrounding the invaded region, as a result of the non-negligible time required to dissipate pressure in the viscous defending fluid.

We are interested in the effect of heterogeneity on the flow pattern. The advancement of the interface is determined by the competition among different pores along the front, which depends on the distribution of throat apertures and pore pressures. We expect the transition from capillary to viscous fingering to occur when the characteristic macroscopic viscous pressure drop "perpendicular" to the interface, $\delta p_\perp$, exceeds the variation in capillary entry pressures along the front, $\delta p_\parallel$. We express $\delta p_\perp\sim\nabla p_\perp L$, where L is the macroscopic length scale, and use Darcy's law $\nabla p_\perp\sim\mu v/k$ to obtain $\delta p_\perp\sim\mu v L/a^2$. We use a fixed value of the macroscopic length scale with $L\gg a$ for the viscous pressure drop in the defending phase, an assumption that is justified during the initial stages of the invasion, but that becomes questionable at later stages, when the invasion front approaches the system's boundaries and becomes fractal [30]. The maximum capillary pressure difference along the front is $\delta p_\parallel=\gamma/r_{\rm min}-\gamma/r_{\rm max}\sim[\lambda/(1-\lambda^2)]\gamma/a$. Equating $\delta p_\perp\sim\delta p_\parallel$, and using the definition of the capillary number, Ca$=\mu v/\gamma$, we predict a transition from VF to CF at Ca$\sim[\lambda/(1-\lambda^2)]a/L$.

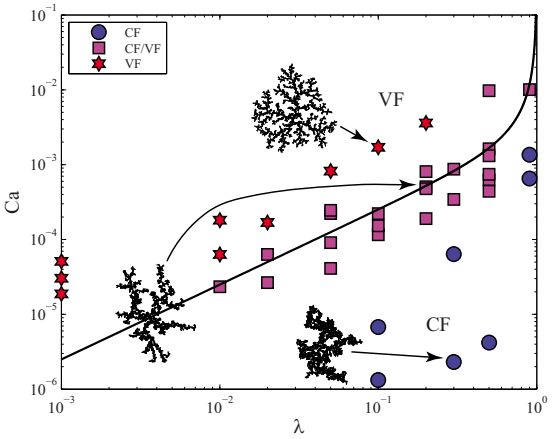

FIG. 2. (Color online) Phase diagram of the invasion pattern as a function of the capillary number Ca and the pore-scale disorder λ, in a rigid solid matrix. The classification is based on visual appearance (see insets), as well as the mass fractal dimension D_f. Box counting [31] provides estimates of $D_f \approx 1.82$ and $D_f \approx 1.64$ for capillary fingering (CF) and viscous fingering (VF), respectively, with standard deviation $\sigma_{D_f}=0.08$ [see the Appendix]. The transition from capillary to viscous fingering (CF/VF) occurs at $\mathrm{Ca} \approx [\lambda/(1-\lambda^2)]a/L$ (black solid line), reflecting a balance between viscosity and pore-scale disorder in capillary entry pressures.

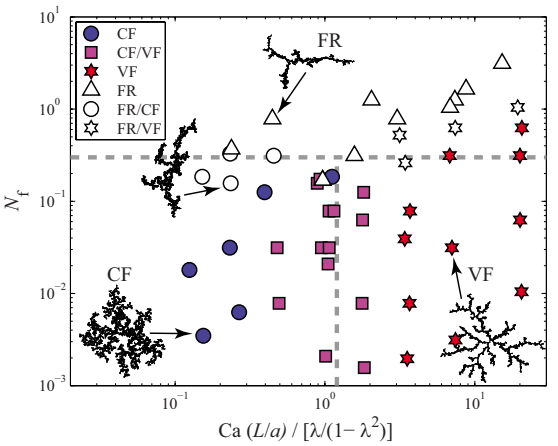

FIG. 3. (Color online) Phase diagram of drainage in deformable disordered media, showing three distinct invasion patterns: viscous fingering (VF), capillary fingering (CF), and fracturing (FR). The gray dashed lines denote transitions among the different regimes. Intermediate regimes are marked by CF/VF, FR/VF, and FR/CF. The deformability of the system is characterized by the fracturing number N_f: drainage is dominated by fracturing in systems with $N_f \gg 1$. At lower N_f values, a transition between CF and VF occurs around $\mathrm{Ca}(L/a)/[\lambda/(1-\lambda^2)] \approx 1$.

We synthesize our results on a phase diagram in the Ca-λ space (Fig. 2). The invasion patterns are classified by visual appearance, as well as by the fractal dimension D_f (see the Appendix). The value of D_f by itself is insufficient to provide unequivocal classification due to expected fluctuations for finite samples. The simulations confirm our predictions on the transition from capillary to viscous fingering. For $\mathrm{Ca}/\lambda \gg a/L$ the effect of heterogeneity is negligible relative to that of Laplacian-driven growth [31], allowing the most advanced fingers to continue propagating. This results in long and thin fingers typical of VF. For $\mathrm{Ca}/\lambda \ll a/L$, the heterogeneity in throat apertures dominates, leading to invasion that propagates at alternating locations. As a result, different parts of the front will coalesce and trap some of the defending fluid behind, creating the fat clusters with thick fingers characteristic of CF.

The two regimes are separated by an intermediate regime centered on the theoretical curve $\mathrm{Ca} \sim [\lambda/(1-\lambda^2)]a/L$. In the limit $\lambda \to 1$ the capillary disorder blows up. The analysis above indeed suggests that the CF regime always dominates in this limit (the crossover curve diverges in the Ca-λ space). In the limit of nearly homogeneous media and high capillary number (not shown in Fig. 2), the model's anisotropy becomes dominant, and dendritic growth occurs along the lattice axes, similar to the experimental results in [7]. Our analysis suggests the existence of a crossover length scale $L_\times \sim [\lambda/(1-\lambda^2)]\mathrm{Ca}^{-1}\, a$, at which the displacement experiences a regime shift from CF (below $L_\times$) to VF (above $L_\times$). A similar conclusion was drawn from the mass fractal dimension of the pattern in drainage experiments [10].

A compliant solid matrix can deform in drainage, which in turn may lead to fracture opening during fluid invasion. Here, we investigate the impact of system deformability on the emergence of invasion patterns. Particle displacements cause changes in the contraction of the springs over time, $h(t)$. To highlight the effect of disorder in flow properties, we assume that the system is initially prestressed homogeneously, such that all springs are subject to the same compression h_0, corresponding to a macroscopic strain $\epsilon_0 = h_0/2a$. Each particle is subject to two types of forces: pressure forces and contact forces. The force exerted on a particle by the fluid occupying an adjacent pore body is oriented at 45° and is of magnitude $f_p = pA_p$, where $A_p \sim a^2$ represents the area upon which the pressure acts. The interparticle contact forces f_c are updated by $f_c(t+\Delta t) = f_c(t) + K\Delta h$, where K is the spring stiffness and $\Delta h = h(t+\Delta t) - h(t)$ is the change in spring contraction. Particle positions are determined at the new time step by imposing force balance at every block, $\Sigma(\vec{f}_p + \vec{f}_c) = \vec{0}$, which leads to a linear system of equations to be solved for Δh of every spring. Particle displacements impact fluid flow because they modify the throat apertures. We evaluate changes in throat apertures and in interparticle forces from the particle displacements, in analogy with cubic packing of particles with frictionless Hertzian contacts, such that $\Delta r = -\Delta h(1-\epsilon)/[2\sqrt{1+(1-\epsilon)^2}]$, where $\epsilon = h(t)/2a$, and the spring stiffness $K = 2E^*\sqrt{R^* h}$, where $R^* = a/2$ and E^* is the constrained Young modulus of the particle material [32]. We simulate material behavior that cannot sustain tension and, therefore, a spring is removed when there is net elongation between blocks ($h \leq 0$). A small cohesive force is applied as a regularization parameter. This force is orders of magnitude smaller than the typical pressure force, and we have confirmed that the results are insensitive to the value of this cohesive force, as long as it is small.

Our model predicts fracturing patterns that are strikingly similar to those observed in 2D experiments, with thin long features which are straight over a length much larger than a

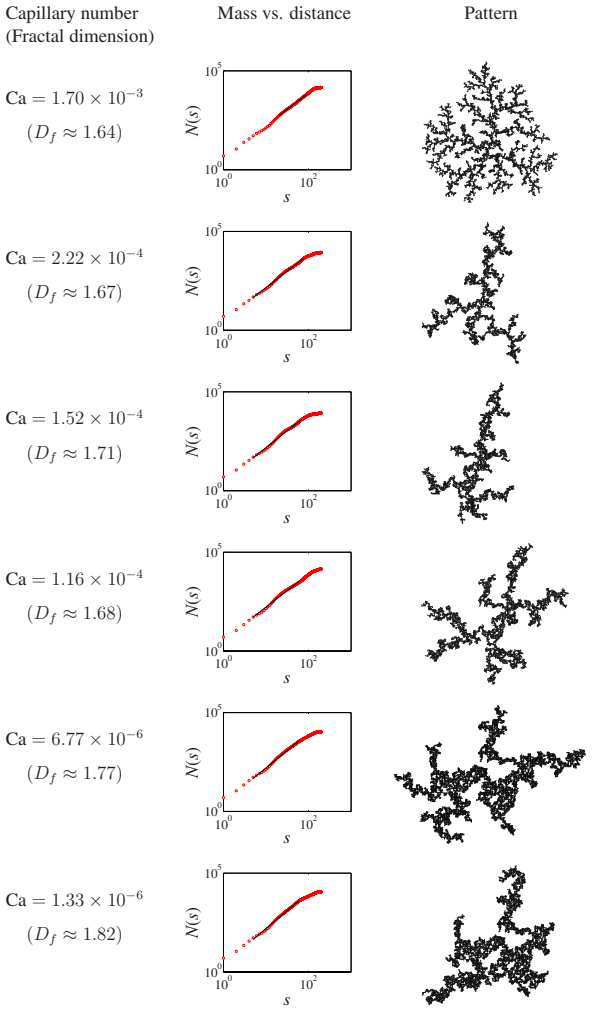

FIG. 4. (Color online) Fractal dimension and displacement pattern for rigid medium, with a value of $\lambda=0.1$, showing a transition from VF to CF as the capillary number is reduced.

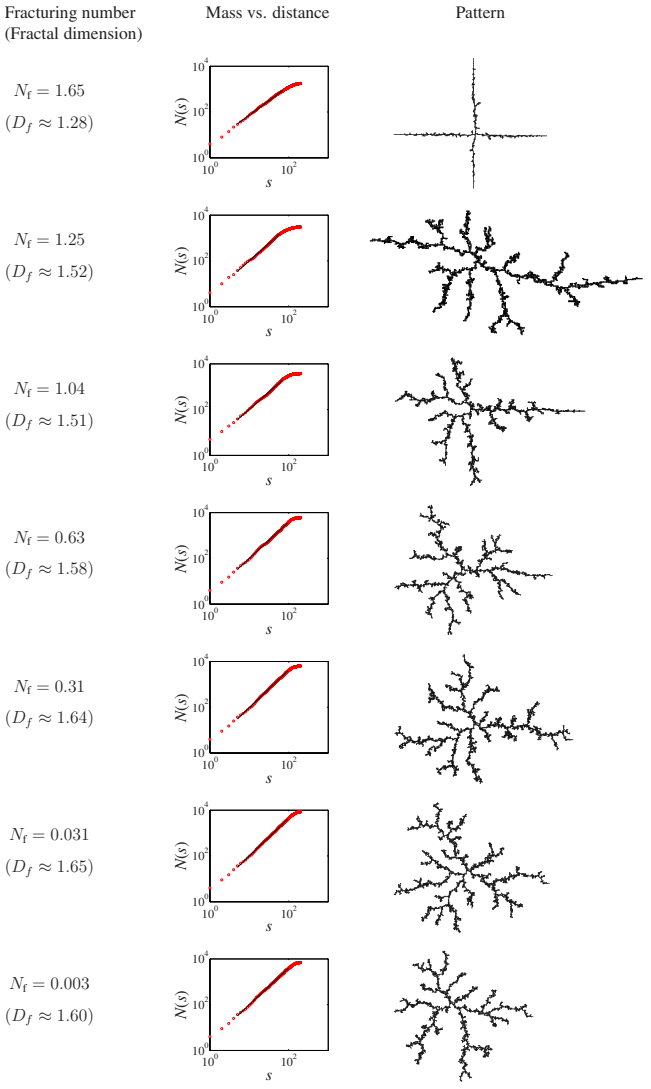

FIG. 5. (Color online) Fractal dimension and displacement pattern for deformable medium, with a value of $\mathrm{Ca}^{*}\approx 10$, showing a transition from fracturing to fingering as the fracturing number is reduced.

pore size [11], and fractal dimension lower than in fingering, $D_f \approx 1.43$ (see the Appendix). The straight segments of the invasion pattern form as a result of localized rearrangements: increasing throat aperture by displacing particles in a direction perpendicular to that of the finger advancement promotes finger growth in that direction. This mechanism is arrested when the front reaches a bottleneck, associated with either initial disorder or compaction ahead of another propagating fracture.

The emergence of a fracturing pattern requires sufficiently large change in throat apertures. Particle rearrangements depend on the balance between the forces applied by the fluids and the interparticle forces holding the particles in place. We define a dimensionless "fracturing number" N_{f} as the ratio of the typical pressure force increment after drainage of a pore, $\Delta f_p \sim \gamma a$, and the force increment resulting from interparticle deformation, $\Delta f_c \sim \lambda E^{*} a^2 \epsilon_0^{1/2}$. The latter is obtained from the condition $\Delta h \sim \Delta r$, where the required change in throat aperture is $\Delta r \sim \lambda \bar{r} \sim \lambda a$, and using the initial overlap h_0 to compute the interparticle stiffness K. With that,

$$N_{\mathrm{f}} = \frac{\gamma}{\lambda a E^{*} \epsilon_0^{1/2}}. \tag{2}$$

An alternative expression for N_{f} is obtained by substituting the initial confining stress $\sigma_0 \sim E^{*} \epsilon_0^{3/2}$ into Eq. (2).

We synthesize drainage behavior in a deformable medium in a phase diagram with two dimensionless groups: the fracturing number N_{f} and a modified capillary number $\mathrm{Ca}(L/a)/[\lambda/(1-\lambda^2)]$ (see Fig. 3). For a rigid medium ($N_{\mathrm{f}} \ll 1$), the transition from capillary to viscous fingering occurs at $\mathrm{Ca}(L/a)/[\lambda/(1-\lambda^2)] \approx 1$. Fracturing is evident when $N_{\mathrm{f}} \gg 1$. A crossover from fingering to fracturing occurs at $N_{\mathrm{f}} \approx 1$. Equation (2) implies that fractures tend to open in fine-particle media, suggesting that below a critical particle size—which decreases with the particle stiffness and the external confinement—invasion is dominated by fracturing. This is consistent with observations of gas bubble growth in sediments [21,22] and drying in porous media [23].

In conclusion, this study explains the crossover among the different fluid displacement patterns of drainage in a deformable medium. The invasion behavior depends on two dimensionless groups. One is related to the influence of pore-scale disorder on the balance between viscous forces and capillary forces. The other measures the deformability of the medium as a function of capillary effects, material properties, and initial confinement. Despite its simplicity, our model predicts the transition from capillary fingering to viscous fingering in rigid media and a crossover from fingering to fracturing in deformable media, suggesting that it captures the essential aspects of the interplay between multiphase fluid flow and mechanical deformation.

This work was supported by the Department of Energy under Grant No. DE-FC26-06NT43067. This financial support is gratefully acknowledged.

APPENDIX

In this appendix we demonstrate the ability of our pore-scale model to capture the transition among the different invasion regimes—VF, CF, and FR. Our classification of the displacement pattern is based on visual appearance, as well as the fractal dimension D_f (using box counting [31]). Visual appearance is an essential consideration in the classification because the estimation of the fractal dimension from the mass vs distance curves is subject to large fluctuations for finite-size systems [5,33–35].

First, we illustrate the transition between VF and CF. For a given value of the disorder parameter, $\lambda=0.1$, we investigate the displacement pattern for a range of capillary numbers. For each value of Ca, we show the displacement pattern and the curve of mass vs distance from which the fractal dimension is obtained (Fig. 4). It is evident that the model predicts a transition from VF (high Ca) to CF (low Ca). Moreover, the values of the fractal dimension are in excellent agreement with experimentally determined values of 1.60–1.65 for VF in a *porous* Hele-Shaw cell [5,34] and the well-known value of 1.82 for invasion-percolation corresponding to CF.

Next, we show the transition between VF and FR by studying displacements with a similar value of the modified capillary number, $\mathrm{Ca}^{*}=\mathrm{Ca}(L/a)/[\lambda/(1-\lambda^2)]\approx 10$, and a range of values of the key dimensionless group, the fracturing number N_{f}. The fracturing pattern is characterized by fingers with straight segments and a lower fractal dimension (Fig. 5).

[1] J. P. Gollub and J. S. Langer, Rev. Mod. Phys. **71**, S396 (1999).
[2] R. Lenormand, E. Touboul, and C. Zarcone, J. Fluid Mech. **189**, 165 (1988).
[3] D. Wilkinson and J. Willemsen, J. Phys. A **16**, 3365 (1983).
[4] L. Paterson, Phys. Rev. Lett. **52**, 1621 (1984).
[5] K. J. Måløy, J. Feder, and T. Jøssang, Phys. Rev. Lett. **55**, 2688 (1985).
[6] J. P. Stokes, D. A. Weitz, J. P. Gollub, A. Dougherty, M. O. Robbins, P. M. Chaikin, and H. M. Lindsay, Phys. Rev. Lett. **57**, 1718 (1986).
[7] J.-D. Chen and D. Wilkinson, Phys. Rev. Lett. **55**, 1892 (1985).
[8] Y. C. Yortsos, B. Xu, and D. Salin, Phys. Rev. Lett. **79**, 4581 (1997).
[9] M. Ferer, C. Ji, G. S. Bromhal, J. Cook, G. Ahmadi, and D. H. Smith, Phys. Rev. E **70**, 016303 (2004).
[10] R. Toussaint, G. Løvoll, Y. Méheust, K. J. Måløy, and J. Schmittbuhl, EPL **71**, 583 (2005).
[11] C. Chevalier, A. Lindner, M. Leroux, and E. Clement, J. Non-Newtonian Fluid Mech. **158**, 63 (2009).
[12] X. Cheng, L. Xu, A. Patterson, H. M. Jaeger, and S. R. Nagel, Nat. Phys. **4**, 234 (2008).
[13] P. Meakin, Science **252**, 226 (1991).
[14] B. Sandnes, H. A. Knudsen, K. J. Måløy, and E. G. Flekkøy, Phys. Rev. Lett. **99**, 038001 (2007).
[15] E. Lemaire, P. Levitz, G. Daccord, and H. Van Damme, Phys. Rev. Lett. **67**, 2009 (1991).
[16] A. Lindner, P. Coussot, and D. Bonn, Phys. Rev. Lett. **85**, 314 (2000).
[17] P. Meakin, G. Li, L. M. Sander, E. Louis, and F. Guinea, J. Phys. A **22**, 1393 (1989).
[18] A. Levermann and I. Procaccia, Phys. Rev. Lett. **89**, 234501 (2002).
[19] F. Tzschichholz and H. J. Herrmann, Phys. Rev. E **51**, 1961 (1995).
[20] K.-t. Leung and Z. Néda, Phys. Rev. Lett. **85**, 662 (2000).
[21] A. K. Jain and R. Juanes, J. Geophys. Res. **114**, B08101 (2009).
[22] B. P. Boudreau, C. Algar, B. D. Johnson, I. Croudace, A. Reed, Y. Furukawa, K. M. Dorgan, P. A. Jumars, and A. S. Grader, Geology **33**, 517 (2005).
[23] L. Xu, S. Davies, A. B. Schofield, and D. A. Weitz, Phys. Rev. Lett. **101**, 094502 (2008).
[24] P. G. de Gennes, Rev. Mod. Phys. **57**, 827 (1985).
[25] W. B. Haines, J. Agric. Sci. **20**, 97 (1930).
[26] K. J. Måløy, L. Furuberg, J. Feder, and T. Jøssang, Phys. Rev. Lett. **68**, 2161 (1992).
[27] L. Furuberg, K. J. Måløy, and J. Feder, Phys. Rev. E **53**, 966 (1996).
[28] E. Aker, K. J. Måløy, and A. Hansen, Phys. Rev. E **58**, 2217 (1998).
[29] C.-H. Lam, Phys. Rev. Lett. **92**, 254503 (2004).
[30] R. Lenormand, Proc. R. Soc. London, Ser. A **423**, 159 (1989).
[31] L. Niemeyer, L. Pietronero, and H. J. Wiesmann, Phys. Rev. Lett. **52**, 1033 (1984).
[32] K. L. Johnson, *Contact Mechanics* (Cambridge University Press, Cambridge, England, 1987).
[33] M. Blunt and P. King, Phys. Rev. A **42**, 4780 (1990).
[34] G. Løvoll, Y. Méheust, R. Toussaint, J. Schmittbuhl, and K. J. Måløy, Phys. Rev. E **70**, 026301 (2004).
[35] O. Praud and H. L. Swinney, Phys. Rev. E **72**, 011406 (2005).